

Asteroseismology of KIC 8263801:

Is it a member of NGC 6866 and a red clump star?

Yanke Tang^{1,2,7}★, Sarbani Basu²★, Guy R. Davies³, Earl P. Bellinger^{4,2,5,6}, Ning Gai^{1,2,7}

¹ *College of Physics and Electronic information, Dezhou University, Dezhou 253023, China*

² *Department of Astronomy, Yale University, P.O. Box 208101, New Haven, CT 06520-8101, USA*

³ *School of Physics and Astronomy, University of Birmingham, Birmingham, B15 2TT, United Kingdom*

⁴ *Max-Planck-Institut für Sonnensystemforschung, Justus-von-Liebig-Weg 3, 37077 Göttingen, Germany*

⁵ *Stellar Astrophysics Centre, Department of Physics and Astronomy, Aarhus University, Ny Munkegade 120, DK-8000 Aarhus C, Denmark*

⁶ *Institut für Informatik, Georg-August-Universität Göttingen, Goldschmidtstrasse 7, 37077 Göttingen, Germany*

⁷ *Shandong Provincial Key Laboratory of Biophysics, Dezhou University, Dezhou 253023, China*

★ *Corresponding authors, email: tyk@dzu.edu.cn; sarbani.basu@yale.edu; ning.gai@hotmail.com*

ABSTRACT

We present an asteroseismic analysis of the *Kepler* light curve of KIC 8263801, a red-giant star in the open cluster NGC 6866 that has previously been reported to be a helium-burning red-clump star. We extracted the frequencies of the radial and quadrupole modes from its frequency power spectrum and determined its properties using a grid of evolutionary models constructed with MESA. The oscillation frequencies were calculated using the GYRE code and the surface term was corrected using the Ball & Gizon (2014) prescription. We find that the star has a mass of $M/M_{\odot} = 1.793 \pm 0.072$, age $t = 1.48 \pm 0.21$ Gyr and radius $R/R_{\odot} = 10.53 \pm 0.28$. By analyzing the internal structure of the best-fitting model, we infer the evolutionary status of the star KIC 8263801 as being on the ascending part of the red giant branch, and not on the red clump. This result is verified using a purely asteroseismic diagnostic, the $\epsilon_c - \Delta\nu_c$ diagram which can distinguish red giant branch stars from red clump stars. Finally, by comparing its age with NGC 6866 ($t = 0.65 \pm 0.1$ Gyr) we conclude that KIC 8263801 is not a member of this open cluster.

Subject headings: stars: evolution – stars: red giant – stars: oscillations

1. Introduction

Since the NASA *Kepler* spacecraft was successfully launched in March 2009, stellar pulsations of over 10,000 red giants have been observed (Borucki et al. 2009, 2010; De Ridder et al. 2009; Bedding et al. 2010; Koch et al. 2010; Gilliland et al. 2010; Balona et al. 2013a,b; Abedigamba 2016). The red giant (RG) star KIC 8263801 is one of these. Located in the field of NGC 6866—the youngest of the four clusters observed by *Kepler*—the pulsations of KIC 8263801 have been observed with a signal-to-noise ratio that is good enough to constrain its fundamental parameters. Balona et al. (2013b) identified 704 stars in this cluster, of which 23 are RG stars showing solar-like oscillations. Abedigamba (2016) used median gravity-mode period spacings (ΔP) to search for red clump (RC) stars among the RG stars showing solar-like oscillations. Based on its $\Delta P = 173.7 \pm 6.4$ s, Abedigamba (2016) determined that KIC 8263801 is a secondary red clump (SRC) star, which is massive enough to have ignited helium burning in a non-degenerate core. However, the signal-to-noise of KIC 8263801 is not enough to derive an accurate ΔP . In this paper, we perform an asteroseismic analysis of the mode frequencies in order to determine the evolutionary state of KIC 8263801.

One of the major problems in the study of open clusters is to determine which stars are members of the clusters and which stars are not. Although, KIC 8263801 has been classified as non-member of NGC 6866 based on photometric distance membership determination and proper motions (Balona et al. 2013b), Balona et al. (2013b) and Abedigamba (2016) pointed out that they can not be quite sure of the membership with only a single method. Abedigamba (2016) stated that NGC6866 is roughly located in the direction of solar apex, which means that all stars (members and non-members) have similar proper motion. one cannot use proper motion to discriminate between members and non-members. No radial velocity measurements for stars located in the field of NGC6866 are available to help in discriminating between members and non-members. The only method left in discriminating between members and non-members in the field of NGC6866 is the photometric distance method. However, with only a single method one cannot be quite sure of the membership. Balona et al. (2013) also attempted to identify cluster members using their proper motions but found very poor discrimination between members and non-members. Hence, another focus of this paper is thus to revisit the issue of the cluster non-membership of KIC 8263801 by means of comparing the age of the star determined through asteroseismic modelling and the age of the cluster.

Asteroseismology is an efficient tool for studying the internal structures of stars through their global oscillations (Tang et al. 2008a,b; Tang & Gai 2011; Chaplin et al. 2011, 2014a,b; Pinsonneault et al. 2014; Silva Aguirre et al. 2015, 2017; Bellinger et al. 2016, 2017). Ba-

stellar properties such as mass, age can be derived this way (e.g., Basu et al. 2010a,b; Yildiz et al. 2017). For the stars with solar-like oscillations, when the signal-to-noise ratios in the seismic data are insufficient to allow robust extraction of individual oscillation frequencies, it is still possible to extract estimates of the large frequency separation ($\Delta\nu$) and the frequency of maximum oscillation power (ν_{\max}). The large separation $\Delta\nu$ is the separation between oscillation modes with the same angular degree and consecutive radial orders (Tassoul 1980):

$$\Delta\nu_l(n) = \nu_{n,l} - \nu_{n-1,l} \quad (1)$$

which scales to a very good approximation with the square root of the stellar mean density (Kjeldsen & Bedding 1995; Stello et al. 2011):

$$\frac{\Delta\nu}{\Delta\nu_{\odot}} \simeq \sqrt{\frac{M/M_{\odot}}{(R/R_{\odot})^3}}. \quad (2)$$

The other, ν_{\max} , is related with the cut-off frequency for acoustic waves in an isothermal atmosphere, which scales with surface gravity g and effective temperature T_{eff} (Brown et al. 1991; Kjeldsen & Bedding 1995) as:

$$\frac{\nu_{\max}}{\nu_{\max\odot}} \simeq \left(\frac{g}{g_{\odot}}\right) \left(\frac{T_{\text{eff}}}{T_{\text{eff},\odot}}\right)^{-1/2} \quad (3)$$

with the solar values $\Delta\nu_{\odot} = 135 \mu\text{Hz}$ and $\nu_{\max\odot} = 3090 \mu\text{Hz}$ (Huber et al. 2009, 2011; Chaplin et al. 2014a) providing the absolute calibration in this study. These scaling relations have been applied with success to main-sequence and sub-giant stars as well as to stars on the red giant branch (RGB) and helium burning (HeB) stars. According to the above scaling relations, asteroseismology can help constrain the global parameters of a star with reasonable precision. For more evolved stars, the scaling relation has reduced accuracy (Gualme et al. 2016; Guggenberger et al. 2016, 2017).

The classical Hertzsprung-Russell diagram (HRD) shows that red giant branch (stars burning hydrogen in a shell around an inert helium core) and red clump (stars with Helium-core and hydrogen-shell burning) occupy overlapping parameter spaces (e.g. Elsworth et al. 2017). Although these stars have different internal conditions, which we can observe indirectly, they have similar surface characteristics—such as effective temperature, surface gravity and total luminosity, which can be observed directly. Hence, from classical observations such as these, it is often not possible to distinguish between RGB stars of about 10-12 R_{\odot} and HeB stars of a similar radius. The distinction is easier in clusters, but even in clusters there is room for ambiguity. This is where asteroseismology is useful. Space missions such as *Kepler* have made red-giant asteroseismology possible, with *Kepler* providing long

time series data that allow the frequency resolution needed to determine frequencies of individual oscillation modes of red giants (Bedding et al. 2011; Beck et al. 2011; Kallinger et al. 2012; Handberg & Lund 2017). Non-radial modes in red giants exhibit mixed character; they behave like gravity modes (g modes) in the interior but like acoustic modes (p modes) in the outer layers. The asteroseismic properties of RGB and HeB stars are quite different (Bedding et al. 2011; Kallinger et al. 2012; Elsworth et al. 2017) and hence are useful in determining the evolutionary state of red giants. This what we do in this paper. We extract the mode frequencies of the radial and quadrupole modes KIC 8263801, construct models that match the frequencies and use those to identify the evolutionary state of the star to determine whether or not it is a member of NGC 6866. Additionally, we also use a purely asteroseismic diagnostic to confirm its evolutionary state. We do not use the dipole modes since the frequencies and frequency spacings of the most g-type modes are determined by the details of the profile of the buoyancy frequency which depends on uncertain model parameters such as the exact treatment of overshoot etc. Radial ($l = 0$) and quadrupole ($l = 2$) mode frequency are more robust in this respect.

In this paper, we extract the mode frequencies of the radial and quadrupole modes by ‘peak bagging’ the frequency power spectrum observed by *Kepler* in § 2. We use these individual mode frequencies to constrain models of KIC 8263801, identify the evolutionary state of the star, and confirm that it is not a member of the open cluster NGC 6866 in § 3 and § 4. Conclusions are presented in § 5.

2. Observational data

2.1. Asteroseismic fitting

We extract the mode frequencies of the radial and quadrupole modes using the KASOC unweighted power spectrum (Handberg & Lund 2014) containing the Kepler data spanning Quarters 1-3, 6-11, and 14 shown in Figure 1. The data result in a frequency resolution of ≈ 9 nHz. First guesses to the frequencies of the radial and quadrupole modes were obtained using a fit of the asymptotic expression for radial modes to the power spectrum (Davies & Miglio 2016). Peakbagging for these modes was done using the procedure, and the code, of Davies et al. (2016). As is described in Davies et al. (2016), an unsupervised machine-learning Bayesian scheme is used to obtain a set of probabilities to assess whether or not a mode had been detected in the data. We use the ratio of the probability of a detection over the probability of no detection (the Bayes factor). If the natural log of the Bayes factor is high, we accept the mode. Only 5 radial orders passed the quality test. The fitted frequencies are given in Table 1. We derive the values of large separation $\Delta\nu = 5.35 \pm 0.01 \mu\text{Hz}$ and

$\nu_{max} = 56.2 \pm 0.4 \mu Hz$ shown in Table 2, which are consistent with the results obtained by Abedigamba (2016).

2.2. Classical observations

The effective temperature $T_{\text{eff}} = 4766$ K, metallicity $[\text{Fe}/\text{H}] = 0.016$ dex, and surface gravity $\log g = 2.487$ (dex) of KIC 8263801 were obtained from Brown et al. (2011). The stated uncertainties of these quantities were 200 K in T_{eff} and 0.4 dex in $\log g$. Although an uncertainty for the metallicity was not reported, the uncertainties were expected to be high. Huber et al. (2014) subsequently presented revised stellar properties for 196 468 *Kepler* targets, including this one. They give $T_{\text{eff}} = 4974 \pm 161 K$, metallicity $[\text{Fe}/\text{H}] = 0.016 \pm 0.30$ (dex), and $\log g = 2.662 \pm 0.03$ for this star. We use these observational constraints as the error boxes as shown in Figure 3, where maximum (black) uncertainty corresponds to the observational value from the *Kepler* website and minimum (green) uncertainty corresponds to the observational value given by Huber et al. (2014). Due to the location of KIC 8263801 in the field of NGC 6866, we also consider that it may have a similar metallicity to this cluster. Bostanci et al. (2015) and Balona et al. (2013b) give the metallicity of the cluster as being about solar value, whereas Loktin et al. (1994) derived $[\text{Fe}/\text{H}] = 0.10$ (dex) via photometry from Hoag et al. (1961). All non-asteroseismic observational constraints are listed in Table 3.

3. Modelling KIC 8263801

3.1. Constructing models

Having values of ν_{max} , $\Delta\nu$ and T_{eff} , the scaling relations (Equations 2 and 3) can be used to calculate the mass, luminosity, and radius of the star. Using these scaling relations, Abedigamba (2016) determined that KIC 8263801 has a mass of $M/M_{\odot} = 1.86$ and luminosity $\log(L/L_{\odot}) = 1.7555$. However, more robust estimates of these quantities can be obtained by means of a grid-based analysis, which constrains stellar parameters by searching among a grid of evolutionary models to get a best fit for observed values of ν_{max} , $\Delta\nu$, T_{eff} and metallicity (e.g., Basu et al. 2010a, 2011; Gai et al. 2011; Chaplin et al. 2014a,b). Since we have extracted the individual frequencies of the star in addition to the global asteroseismic parameters, we can use grid-based modelling to obtain better results by selecting models that fit the observed frequencies and not just the global asteroseismic parameters ν_{max} and $\Delta\nu$.

We use the MESA stellar evolution code (*Modules for Experiments in Stellar Astrophysics*, Paxton et al. 2011, 2013, version 8845) to construct models. We employ the default MESA input options unless otherwise stated. We evolve each pre-main sequence model until its nuclear luminosity first reaches 99.9% of the total luminosity, which we define as being zero-age main sequence (ZAMS). We use the Eddington T- τ atmosphere from ZAMS onwards. Each track is then evolved from ZAMS to asymptotic giant branch (AGB) as shown in Figure 3. We treat the convection zone by the standard mixing-length theory (MLT) of Cox & Giuli (1968) with the mixing-length parameter $\alpha_{\text{MLT}} = 2.0$ (Wu & Li 2016).

Referring to the mass value derived by Abedigamba (2016), we make models in a range of initial masses from $1.7 M_{\odot}$ to $2.0 M_{\odot}$ with a step of $0.02 M_{\odot}$. According to the discussion of metallicity presented in Section 2.2, we allow the initial heavy element abundances Z_i to range from 0.01 to 0.025 with a step of 0.005 as shown in Table 4 via

$$\log[Z/X] \simeq [\text{Fe}/\text{H}] + \log[Z/X]_{\odot}, \quad (4)$$

where $[Z/X]_{\odot} = 0.023$ (Grevesse & Sauval 1998). All input parameters are shown in Table 4. Once the initial heavy element abundance Z_i is determined, the dependence of initial helium mass fraction Y_i on Z_i can be set using a linear helium enrichment expression with the primordial helium abundance $Y_p = 0.24$ and the slope $\Delta Y/\Delta Z = 2$ (Demarque 2004; Basu et al. 2010a) by the following:

$$Y_i = Y_p + \frac{\Delta Y}{\Delta Z} Z_i. \quad (5)$$

Finally, the initial hydrogen element abundance X_i is obtained via

$$X_i = 1 - Y_i - Z_i. \quad (6)$$

3.2. Calculating mode frequencies

We use the GYRE oscillation code (Townsend & Teitler 2013) to calculate the mode frequencies of the models. Due to surface effects, there is a systematic offset between the observed and model frequencies (e.g. Christensen-Dalsgaard 1984). In order to obtain the accurate modeling of solar-like oscillations, we should use a systematic shift to correct the model frequencies. A number of ways have been proposed to correct the frequencies for the surface issues (usually called the “surface term” correction). The most common way to correct for the surface term for stellar models is the method proposed by Kjeldsen et al. (2008). They note that offset between observed and best model frequencies turns out to be closely fitted by a power law. However, there are issues with many of the surface term

corrections, even for main sequence stars; and most models perform very badly in the sub-giant and red-giant region. Schmitt & Basu (2015) found that the two-term model proposed by Ball & Gizon (2014) works better than other models across a large portion of the HR diagram, and consequently we adopt that for this work.

4. Results and discussions

We show the evolutionary track of our models in Figure 3. The figure also shows the two error boxes. $T_{\text{eff}} = 4766 \pm 200K$ and $\log g = 2.487 \pm 0.4$ have been used for the large error box while $T_{\text{eff}} = 4974 \pm 161K$ and $\log g = 2.662 \pm 0.03$ for the smaller error box. We find that many models fall in the two error boxes. In order to obtain the best-fit model for KIC 8263801 from among these models, we calculated the likelihood for each model and determined the model with the highest likelihood. The likelihood function is defined as

$$\mathcal{L} = \left(\prod_{i=1}^n \frac{1}{\sqrt{2\pi}\sigma_i} \right) \cdot \exp \left\{ -\frac{\chi^2}{2} \right\} \quad (7)$$

where

$$\chi^2 = \sum_{i=1}^n \left(\frac{q_i^{\text{obs}} - q_i^{\text{model}}}{\sigma_i} \right)^2. \quad (8)$$

with the quantity q_i^{obs} indicating the observed T_{eff} , $[\text{Fe}/\text{H}]$, and frequency $\nu_{n,l}$; while the q_i^{model} corresponds to these values of the model. The quantity σ_i represents the observational error of q_i^{obs} . In the study, we use the function as follows:

$$\mathcal{L}(T_{\text{eff}}, [\text{Fe}/\text{H}], \nu) = \mathcal{L}_{T_{\text{eff}}} \cdot \mathcal{L}_{[\text{Fe}/\text{H}]} \cdot \mathcal{L}_{\nu} \quad (9)$$

where

$$\mathcal{L}_{T_{\text{eff}}} = \frac{1}{\sqrt{2\pi}\sigma_{T_{\text{eff}}}} \cdot \exp \left\{ -\frac{(T_{\text{eff,obs}} - T_{\text{eff,model}})^2}{2\sigma_{T_{\text{eff}}}^2} \right\} \quad (10)$$

$$\mathcal{L}_{[\text{Fe}/\text{H}]} = \frac{1}{\sqrt{2\pi}\sigma_{[\text{Fe}/\text{H}]}} \cdot \exp \left\{ -\frac{([\text{Fe}/\text{H}]_{\text{obs}} - [\text{Fe}/\text{H}]_{\text{model}})^2}{2\sigma_{[\text{Fe}/\text{H}]}^2} \right\} \quad (11)$$

$$\mathcal{L}_{\nu} = \prod_{i=1}^{10} \left(\frac{1}{\sqrt{2\pi}\sigma_i(\nu)} \cdot \exp \left\{ -\frac{(\nu_i^{\text{obs}} - \nu_i^{\text{model}})^2}{2\sigma_i^2(\nu)} \right\} \right). \quad (12)$$

In the above expression, ν_i^{model} are the surface-term corrected frequencies of the models.

The values of likelihood function for model of KIC 8263801 as function of mass, metallicity, age and radius are shown in Figure 4. We choose the model of maximizes \mathcal{L} as a

candidate for the best-fit model. The model parameters are shown in Table 5. To clearly compare all of the theoretical frequencies of the best-fit model with observed frequencies, we show the échelle diagram of the best-fit model in Figure 5. In the figure, open symbols are the model frequencies corrected for the surface term, the filled symbols refer to the observable frequencies. Circles are used for $l = 0$ modes and squares for $l = 2$ modes.

Finally, we derive the parameters of star as the likelihood weighted mean and standard deviation from the models and obtain a mass of $M/M_{\odot} = 1.793 \pm 0.072$, age of $t = 1.48 \pm 0.21$ Gyr and radius of $R/R_{\odot} = 10.53 \pm 0.28$. Our best-fit model has an age of 1.596 Gyr, the age as determined from the likelihood weighted average is not too different, and thus the question arises as to whether this star can be a member of NGC 6866. There are a number of results about the age of NGC 6866. For example, Loktin et al. (1994) derived $t = 0.66$ Gyr; Günes et al. (2012) obtained an age of $t = 0.8 \pm 0.1$ Gyr by 2MASS photometry; Kharchenko (2005) obtained an age of $t = 0.5$ Gyr using isochrone-based procedure; Bostanci et al. (2015) derived $t = 0.813 \pm 0.05$ Gyr with the metallicity of the cluster being about the solar value; Janes et al. (2014) derived age $t = 0.705 \pm 0.170$ Gyr; and Balona et al. (2013b) estimated the age as $t = 0.65 \pm 0.1$ Gyr with isochrones of solar composition. While the age estimates vary considerably, it is clear that the consensus is the age of NGC 6866 is less than 1 Gyr. Our age estimate of KIC 8263801 is significantly higher than 1 Gyr. Based on these results, we could conclude that KIC 8263801 is a non-member of the cluster NGC 6866, which is consistent with Balona et al. (2013b).

We also derived the stellar parameters of KIC 8263801 using the Bayesian tool PARAM (da Silva et al. 2006; Rodrigues et al. 2014, 2017) and the grid models computed with MESA. The mode and its 68 percent credible intervals of the posterior probability density function (PDF) as errors of parameters are mass $M/M_{\odot} = 1.8507^{+0.0721}_{-0.0249}$, age $t = 1.5844^{+0.1046}_{-0.1555}$ Gyr, radius $R/R_{\odot} = 10.5724^{+0.1414}_{-0.1185}$ and $\log g = 2.6544^{+0.003}_{-0.0048}$ dex. These results from PARAM are consistent with our above analysis ($M/M_{\odot} = 1.793 \pm 0.072$, age $t = 1.48 \pm 0.21$ Gyr, radius $R/R_{\odot} = 10.53 \pm 0.28$) within errors, and $\log g = 2.6544^{+0.003}_{-0.0048}$ dex is consistent with observation $\log g = 2.487 \pm 0.04$ dex within uncertainties.

As mentioned above, and as is clear from Figure 3, red giants with inert helium cores and red giants with helium burning cores occupy a common region in the HR diagram. Errors in temperature and metallicity determinations make it difficult to unambiguously determine the evolutionary state, and hence age, of a red giant. Several asteroseismic tools have been developed to distinguish between the stars (Bedding et al. 2011; Kallinger et al. 2012; Elsworth et al. 2017). From the work presented above, we get the the best fit models of KIC 8263801 through modelling. The best fit model of KIC 8263801 is a red giant star which imply that the star in question is on the ascending branch (hence has an inert core).

We use the technique of Kallinger et al. (2012) to confirm the result; the data do not have a high enough signal-to-noise ratio to use the observed $l = 1$ period spacing as suggested by Bedding et al. (2011), but have the signal-to-noise is high enough to be able to determine mode frequencies making it unnecessary to use the method of Elsworth et al. (2017). The fact that we have good estimates of radial-mode frequencies makes the method of Kallinger et al. (2012) ideal.

Kallinger et al. (2012) found that the phase function ϵ determined around ν_{\max} could be used to distinguish between RGB and HeB stars. White et al. (2011) find that the phase shift ϵ changes with the evolutionary state of a star, and Kallinger et al. (2012) pointed out especially the central value of ϵ , which given by the three radial modes around ν_{\max} , contains the necessary information. In this work, we tested all of the above methods and find that considering the central radial modes like Kallinger et al. (2012) is suitable. (Kallinger et al. 2012) expressed the three central radial orders p modes by the following formula:

$$\nu_{c0} = \Delta\nu_c(n + \epsilon'_c), \quad (13)$$

where ν_{c0} is central frequency varying in the range $\nu_{\max} \pm 0.55\Delta\nu$ and $\Delta\nu_c$ is the separation between the three central modes. As explained by Rodrigues et al. (2017), to determine the large frequency properly, we use weighted least squares fit to calculate an average large-frequency separation $\langle\Delta\nu\rangle$. We use a Gaussian function, as described in Mosser et al. (2012) and Rodrigues et al. (2017), to calculate the individual weights:

$$\omega = \exp\left\{-\frac{(\nu - \nu_{\max})^2}{2\sigma^2}\right\} \quad (14)$$

where $\sigma = 0.66 \cdot \nu_{\max}^{0.88}$.

If ν_{c0} and $\Delta\nu_c$ are given, the phase shift of ϵ_c can be determined by the following formula defined by Kallinger et al. (2012):

$$\epsilon_c = \begin{cases} \epsilon'_c + 1 & \text{if } \epsilon'_c < 0.5 \text{ and } \Delta\nu > 3\mu\text{Hz} \\ \epsilon'_c & \text{otherwise} \end{cases} \quad (15)$$

with

$$\epsilon'_c = \left(\frac{\nu_{c0}}{\Delta\nu_c}\right) \bmod 1. \quad (16)$$

In Figure 6, we show the central value of ϵ_c for all the models from red giants to red clump (with $\Delta\nu_c \leq 8\mu\text{Hz}$) along the evolutionary track, which are calculated using the input parameters in Table 4. Figure 6 display the ϵ_c against the large separation between the central modes. The stars clearly divide into different groups, where the circles are RGB

models while the triangles are HeB models. The (blue) square in the figure denotes the observed value of ϵ_c with error bar of the star, obtained by error propagation analysis. We thus find that the KIC 8263801 is indeed an inert-core RGB star. Although Abedigamba (2016) had used the median gravity-mode period spacing ΔP of $l = 1$ modes to determine that KIC 8263801 is a helium-burning secondary red-clump (SRC) star, we believe that the low SNR of the data affected the value of ΔP obtained by them. Given the mass of the best-fit model, ΔP would be the most reliable way of determining the evolutionary state of this star if measured properly (see Bedding et al. 2011). However, KIC 8263801 has a $\Delta\nu_c$ of about $5.35\mu Hz$, and in that region of Figure 6, the two stages of evolution are well separated.

5. Conclusions

We have done an asteroseismic study of the star KIC 8263801 in order to determine its age, evolutionary status and membership or otherwise in the open cluster NGC 6866. Our best fit models has mass $M/M_\odot = 1.76$, age $t = 1.596$ Gyr, radius $R/R_\odot = 10.3483$ while a full grid analysis gives $M/M_\odot = 1.793 \pm 0.072$, age $t = 1.48 \pm 0.21$ Gyr and radius $R/R_\odot = 10.53 \pm 0.28$.

The best fit model of KIC 8263801 is on the ascending part of the red giant branch, making it likely that KIC 8263801 is also in that state. We confirm this using the $\epsilon_c - \Delta\nu_c$ diagram.

The age estimates of KIC 8263801 makes it unlikely to be a member cluster NGC 6866, despite being in the same field since NGC 6866 has age estimates below 1 Gyr. This result is consistent with that of Balona et al. (2013b).

Y.K.T. and N.G. acknowledges the research grant from the National Natural Science Foundation of China (Grant No. 11673005). S.B. acknowledges NSF grant AST-1514676 and NASA grant NNX16AI09G. E.P.B. acknowledges support from the European Research Council under the European Community’s Seventh Framework Programme (FP7/2007-2013) / ERC grant agreement no 338251 (StellarAges) and the National Physical Science Consortium (NPSC) Fellowship.

REFERENCES

Abedigamba, O. P., 2016, *New Astronomy*, 46, 21

- Basu, S., Chaplin, W. J., & Elsworth, Y. 2010a, *ApJ*, 710, 1596
- Basu, S., Chaplin, W. J., & Elsworth, Y. 2010b, *Ap&SS*, 328, 79
- Basu, S., Grundahl, F., Stello, D. et al. 2011, *ApJ*, 729, 10
- Ball, W. H. & Gizon, L. 2014, *A&A*, 568, A123
- Balona, L. A., Medupe, T., Abedigamba, O. P. et al. 2013a, *MNRAS*, 430, 3472
- Balona, L.A., Joshi, S., Joshi, Y.C., Sagar, R. 2013b, *MNRAS*, 429, 1466.
- Bellinger, E. P., Angelou, G. C., Hekker, S., et al. 2016, *ApJ*, 830, 31
- Bellinger, E. P., Angelou, G. C., Hekker, S., et al. 2017, *Seis. Sun & Dist. Stars*, 160, id.05003
- Bedding, T. R., Huber, D., Stello, D. et al. 2010, *ApJL*, 713, L176
- Bedding, T. R., Mosser, B., Huber, D. et al. 2011, *Nature*, 471, 608
- Bedding, T. R., 2014. *Aste.book.60*.
- Beck, P. G., Bedding, T. R., Mosser, B., Stello, D. et al. 2011, *Science*, 332, 205
- Borucki, W., Koch, D., Batalha, N., 2009, *IAUSymposium* 289.
- Borucki, William J.; Koch, David.; Basri, Gibor. et al., 2010, *Science*, 327, 977
- Bostanci, Z. F., Ak, T., Yontan, T., et al. 2015, *MNRAS*, 453, 1095
- Brown, T. M., Gilliland, R. L., Noyes, R. W., Ramsey, L. W., 1991, *ApJ*, 368, 599
- Brown, Timothy M.; Latham, David W.; Everett, Mark E.; Esquerdo, Gilbert A. 2011, *AJ*, 142, 112
- Chaplin, W. J., Kjeldsen, H., Christensen-Dalsgaard, J., et al. 2011, *Sci*, 332, 213
- Chaplin, W. J., Basu, S., Huber, D., et al., 2014a, *ApJS*, 210, 1
- Chaplin, W. J., Elsworth, Y., Davies, G. R., et al. 2014b, *MNRAS*, 445, 946
- Christensen-Dalsgaard, J. 1984, *Space Research in Stellar Activity and Variability*, 11
- Cox, J. P., & Giuli, R. T. 1968, *Principles of Stellar Structure* (New York: Gordon and Breach
- da Silva, L., Girardi, L., Pasquini, L. et al. 2006, *A&A*, 458, 609

- Demarque, P., Woo, J. -H., Kim, Y. -C. & Yi, S. K. 2004, *ApJS*, 155, 667
- De Ridder, J., Barban, C., Baudin, F. et al. 2009, *Nature*, 459, 398
- Davies, G. R., Aguirre, V. S., Bedding, T. R., et al. 2016, *MNRAS*, 456, 2183
- Davies, G. R. & Miglio, A. 2016, *Astronomische Nachrichten*, 337, 774
- Elsworth Y., Hekker S., Basu S., Davies G., 2017, *MNRAS*, 466, 3344
- Gai, N., Basu, S., Chaplin, William, J. & Elsworth, Y. 2011, *ApJ*, 730, 63
- Gilliland, R. L., Brown, T. M., Christensen-Dalsgaard, J. et al. 2010, *PASP*, 122, 131
- Grevesse, N. & Sauval, A. J. 1998, *Space Sci. Rev.*, 85, 161
- Günes O., Karatas Y., Bonatto C., 2012, *NewA*, 17, 720
- Gualme, P., McKeever, J., Jackiewicz, J. et al. 2016, *ApJ*, 832, 121
- Guggenberger, E., Hekker, S., Basu, S. et al. 2016, *MNRAS*, 460, 4277
- Guggenberger, E., Hekker, S., Angelou, G. et al. 2016, *MNRAS*, 470, 2069
- Handberg, R.& Lund, M. N. 2014, *MNRAS*, 445, 2698
- Handberg, R.& Lund, M. N. 2017, *A&A*, 597, id.A36
- Huber, D., Stello, D., Bedding, T. R., et al. 2009, *CoAst*, 160, 74
- Huber, D., Bedding, T. R., Stello, D., et al. 2011, *ApJ*, 743, 143
- Huber, D., Silva Aguirre, V., Matthews, J. M., et al. 2014, *ApJS*, 211, 2
- Hoag A. A., Johnson H. L., Iriarte B., Mitchell R. I., Hallam K. L., Sharpless S., 1961, *Publ. U.S. Naval Obs. (Second Series)*, 17, 1
- Janes K., Barnes S. A., Meibom S., Hoq S., 2014, *AJ*, 147, 139
- Kallinger, T., Hekker, S., Mosser, B. et al. 2012, *A&A*, 541, A51
- Kjeldsen, H., Bedding, T. R., 1995, *A&A*, 293, 87
- Kjeldsen, H., Bedding, T. R. & Christensen-Dalsgaard, J. 2008, *ApJ*, 683, L175
- Koch, D. G., Borucki, W. J., Basri, G. et al. 2010, *ApJ*, 713, L79

- Kharchenko, N. V., Piskunov, A. E., Röser, S., 2005, *A&A*, 438, 1163.
- Loktin A. V., Matkin N. V., Gerasimenko T. P., 1994, *Astron. Astrophys. Trans.*, 4, 153
- Mosser, B., Elsworth, Y., Hekker, S. et al. 2012, *A&A*, 537, A30
- Paxton, B., Bildsten, L., Dotter, A., et al. 2011, *ApJS*, 192
- Paxton, B., Cantiello, M., Arras, P., et al. 2013, *ApJS*, 208
- Pinsonneault, M. H., Elsworth, Y., Epstein, C., et al. 2014, *ApJS*, 215, 19
- Rodrigues T. S., Girardi, L., Miglio, A. et al., 2014, *MNRAS*, 445, 2758
- Rodrigues T. S., Bossini, D., Miglio, A. et al., 2017, *MNRAS*, 467, 1433
- Stello, D., Meibom, S., Gilliland, R. L., et al. 2011, *ApJ*, 739, 13
- Schmitt, J. R. & Basu, S. 2015, *ApJ*, 808, 123
- Silva Aguirre, V., Davies, G. R., Basu, S., et al. 2015, *MNRAS*, 452, 2127
- Silva Aguirre, V., Lund, M. N., Antia, H. M., et al. 2017, *ApJ*, 835, 173
- Tang, Y. K., Bi, S. L., Gai, N., & Xu, H. Y. 2008a, *Chinese J. A&A*, 8, 421
- Tang, Y. K., Bi, S. L., & Gai, N. 2008b, *NewA*, 13, 541
- Tang, Y. K. & Gai, N. 2011, *A&A*, 526, A35
- Tassoul, M., 1980. *ApJS* 43, 469.
- Townsend R. H. D., Teitler S. A., 2013, *MNRAS*, 435, 3406
- White T. R., Bedding T. R., Stello D., Christensen-Dalsgaard J., Huber D., Kjeldsen H., 2011, *ApJ*, 743, 161
- Wu, Tao, & Li, Yan, 2016, *ApJ*, 818, L13
- Yildiz, M., Çelik Orhan, Z., Örtel, S., Roth, M. 2017, *MNRAS*, 470, L25

Table 1: Asteroseismic observational frequencies of KIC 8263801.

n	l	Value	Error
8	0	43.242	0.068
9	0	48.294	0.020
10	0	53.705	0.017
11	0	59.126	0.012
12	0	64.502	0.063
8	2	41.64	0.86
9	2	47.573	0.032
10	2	52.810	0.069
11	2	58.352	0.020
12	2	63.75	0.12

Table 2: Asteroseismic global parameters of KIC 8263801.

Observable Variable	Value	Source
Large separation $\Delta\nu$	5.35 ± 0.01	(1)
	5.3541	(2)
ν_{\max}	56.2 ± 0.4	(1)
	56.422	(2)

References. (1) this paper; (2) Abedigamba (2016).

Table 3: Non-asteroseismic data of KIC 8263801.

Observed Variable	Value	Source
Effective temperature $T_{\text{eff}}(K)$	4766	(1)
	4974 ± 161	(2)
Metallicity [Fe/H]	0.016	(1)
	0.016 ± 0.30	(2)
$\text{Log } g$ (dex)	2.487	(1)
	2.662 ± 0.03	(2)

References. (1) Brown et al. (2011) ; (2) Huber et al. (2014).

Table 4: Input parameters for models

Variable	Minimum Value	Maximum Value	Step Size
Initial Mass (M_{\odot})	1.70	2.00	0.02
Initial heavy element abundance Z_i	0.01	0.025	0.005

Table 5: The parameters of the best-fit model.

Model parameters	Value
Mass (M_{\odot})	1.76
Age (Gyr)	1.596
Effective temperature $T_{\text{eff}}(K)$	4884.3
Luminosity $\log L/L_{\odot}$	1.7384
$\log g$ (dex)	2.654
$\log R/R_{\odot}$	1.01487

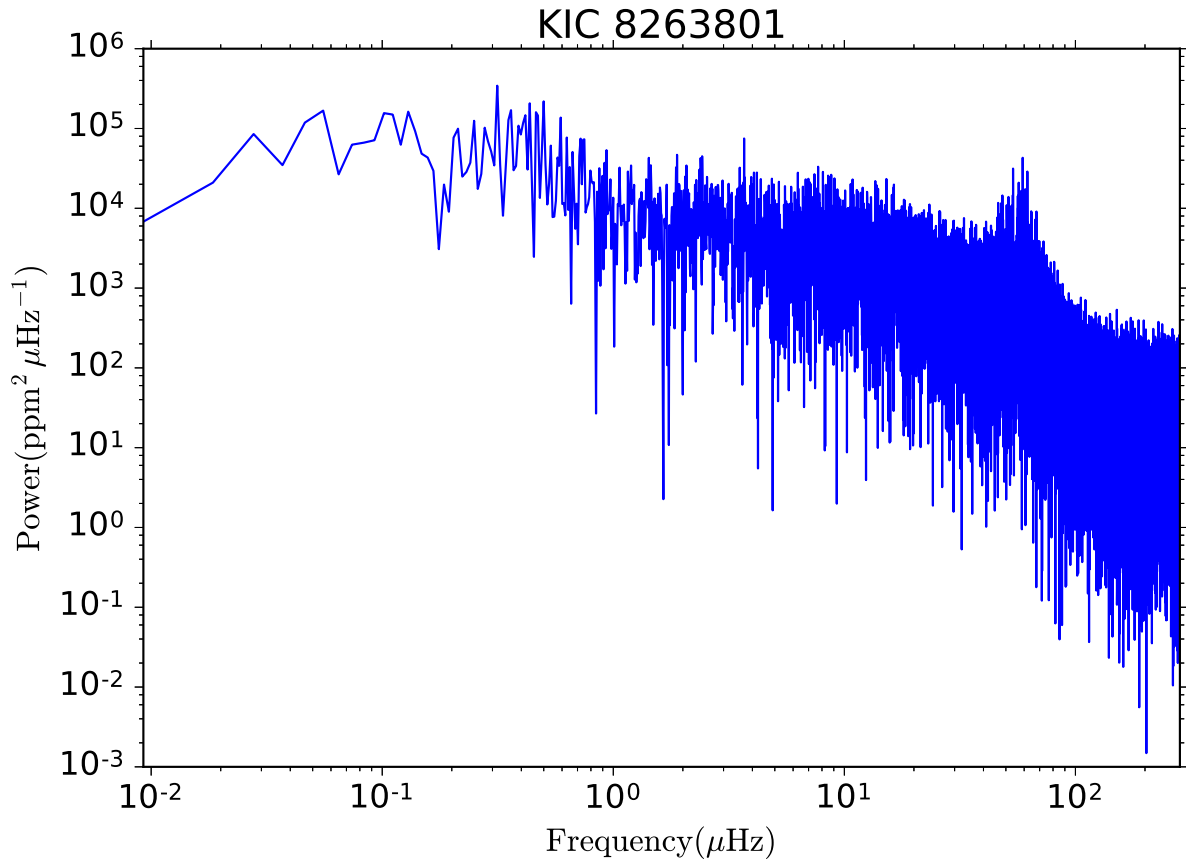


Fig. 1.— The power spectrum for KIC8263801 from *KEPLER* photometry.

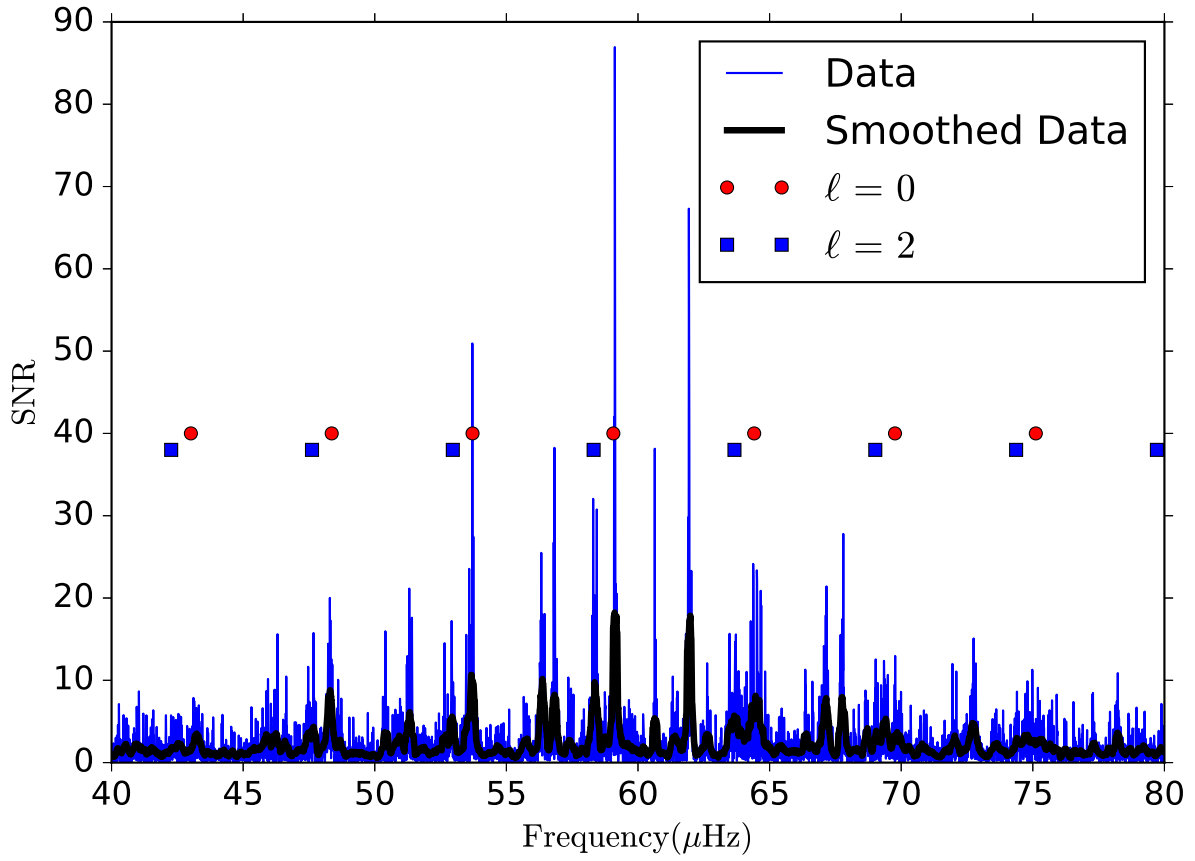


Fig. 2.— Identified p-mode oscillation spectrum of the red giant KIC8263801 in function of frequency. The (blue) thin and (black) thick lines denote the power spectrum before and after smoothing.

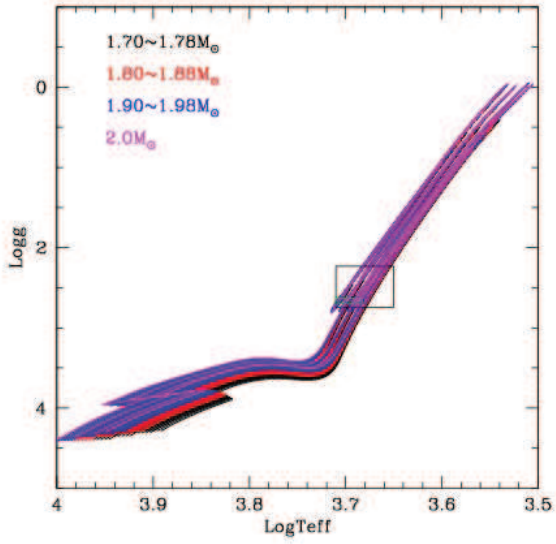


Fig. 3.— Evolutionary tracks of models constructed for this work. The large (black) error box corresponds to observational values from the *Kepler* website, while small (green) error box corresponds to the revised observational value given by Huber et al. (2014)

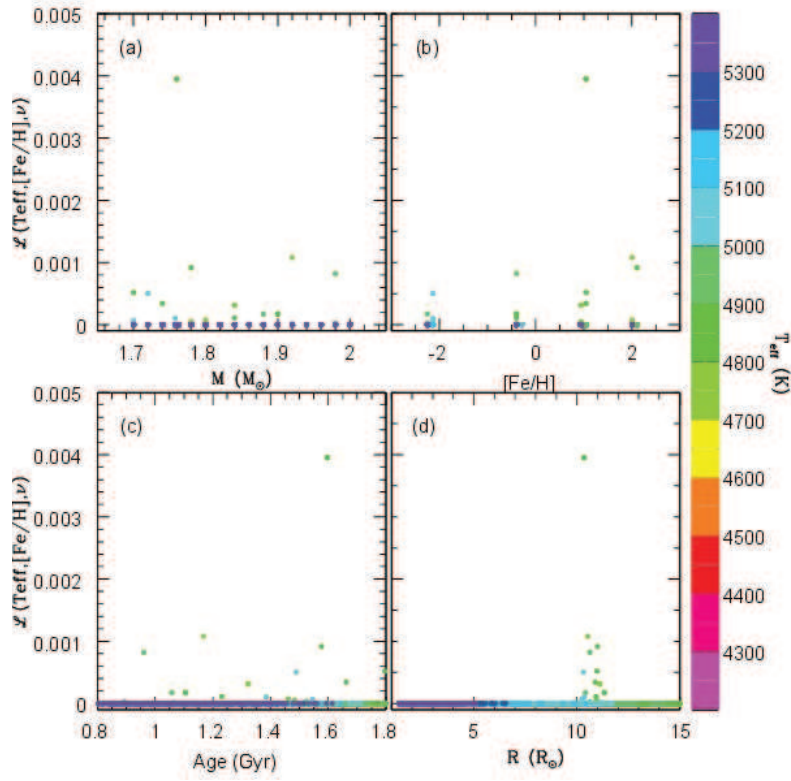


Fig. 4.— The likelihood values for models of KIC 8263801 as function of mass, metallicity, age and radius, corresponding to panel (a), (b), (c) and (d) respectively.

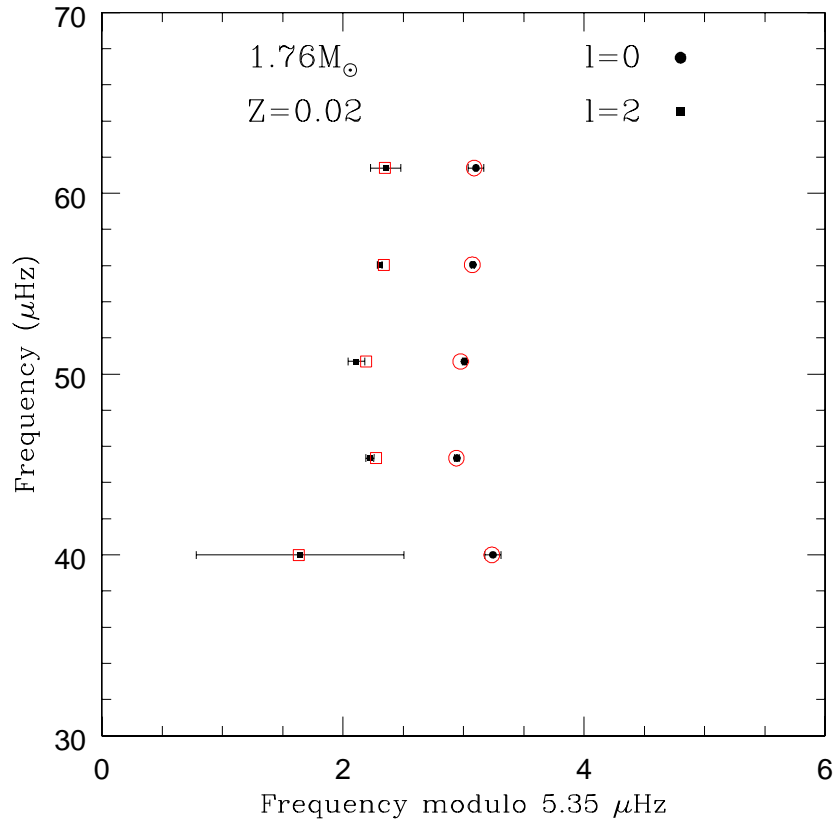


Fig. 5.— Échelle diagrams for the best-fit model. Open symbols are the surface-term corrected frequencies of the best-fit model; filled symbols refer to the observed frequencies. Circles are used for $l = 0$ modes, squares for $l = 2$ modes.

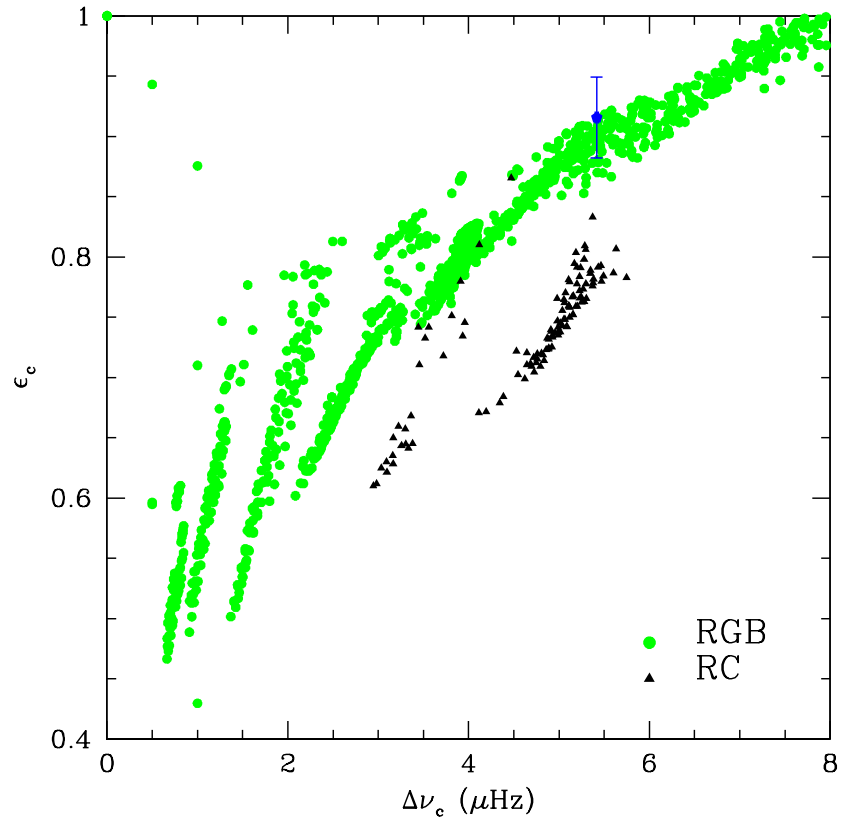


Fig. 6.— Central value of ϵ_c for models plotted against the large separation between the central modes. The (green) filled circles are RGB models, while the (black) filled triangles are RC models. The (blue) filled square with error-bars is observed result for KIC 8263801.